

Hot Exciton Effect in Photoluminescence of Monolayer Transition Metal Dichalcogenide

Ke Xiao¹, Ruihuan Duan², Zheng Liu², Kenji Watanabe³, Takashi Taniguchi³, Wang Yao¹, and Xiaodong Cui¹

¹The University of Hong Kong

²Nanyang Technological University

³National Institute for Materials Science

July 11, 2022

Abstract

Hot excitons are usually neglected in optical spectroscopy in 2D semiconductors for the sake of momentum conservation, as the majority of hot excitons are out of light cones. In this letter, we elaborate the contribution of hot excitons to optical properties of monolayer MoSe₂ with photoluminescence (PL) and photoluminescence excitation (PLE) spectroscopy. With the excitation-intensity-dependent PL, temperature-dependent PL and PLE experiments combined with the simulations, we experimentally distinguish the influences of the exciton temperature and the lattice temperature in the PL spectrum. It is concluded that the acoustic phonon assisted photoluminescence accounts for the non-Lorentzian high energy tail in the PL spectrum and the hot exciton effect is significant to linear optical properties of TMDs. Besides, the effective exciton temperature is found to be several tens of Kelvin higher than the lattice temperature at non-resonant optical excitation. It indicates that the exciton temperature needs to be carefully taken into account when considering the exciton related quantum phase phenomena such as exciton condensation. It is experimentally demonstrated that the effective exciton temperature can be tuned by excitation energy.

Hot Exciton Effect in Photoluminescence of Monolayer Transition Metal Dichalcogenide

Ke Xiao¹, Ruihuan Duan², Zheng Liu², Kenji Watanabe³, Takashi Taniguchi⁴, Wang Yao¹, Xiaodong Cui¹, *

¹ Department of Physics, University of Hong Kong, Hong Kong SAR

² School of Materials Science and Engineering, Nanyang Technological University, Singapore 639798, Singapore

³ Research Center for Functional Materials, National Institute for Materials Science, 1-1 Namiki, Tsukuba 305-0044, Japan

⁴ International Center for Materials Nanoarchitectonics, National Institute for Materials Science, 1-1 Namiki, Tsukuba 305-0044, Japan

* e-mail: xdcui@hku.hk

Abstract

Hot excitons are usually neglected in optical spectroscopy in 2D semiconductors for the sake of momentum conservation, as the majority of hot excitons are out of light cones. In this letter, we elaborate the contribution of hot excitons to optical properties of monolayer MoSe₂ with photoluminescence (PL) and photoluminescence excitation (PLE) spectroscopy. With the excitation-intensity-dependent PL, temperature-dependent

PL and PLE experiments combined with the simulations, we experimentally distinguish the influences of the exciton temperature and the lattice temperature in the PL spectrum. It is concluded that the acoustic phonon assisted photoluminescence accounts for the non-Lorentzian high energy tail in the PL spectrum and the hot exciton effect is significant to linear optical properties of TMDs. Besides, the effective exciton temperature is found to be several tens of Kelvin higher than the lattice temperature at non-resonant optical excitation. It indicates that the exciton temperature needs to be carefully taken into account when considering the exciton related quantum phase phenomena such as exciton condensation. It is experimentally demonstrated that the effective exciton temperature can be tuned by excitation energy.

Introduction:

Monolayer transition metal dichalcogenides (TMDs) has been recognized as one of superior playgrounds for two-dimensional (2D) physics, particularly 2D exciton study. The weak Coulomb screening and 2D nature lead to prominent excitons with a giant binding energy dominating monolayer TMDs' optical properties^{1, 2, 3, 4, 5, 6}. The attributes of excitons in monolayer TMDs featuring strong oscillator strength, richness of degrees of freedom, i.e. spin and valley, and spin-valley locking^{7, 8} have been stimulating intriguing experiments in many-body physics.^{9, 10} Especially, the strong spin-orbit coupling of the transition metal atoms gives rise to the large spin splitting in valence band, resulting in the two families of optical accessible bright excitons, namely A excitons (lower energy) and B excitons (higher energy).^{11, 12} As yet not much attention has been paid to the influence of hot excitons whose kinetic energy is significantly higher than lattice temperature. Unlike hot electrons which affect physics properties in many aspects^{13, 14, 15}, hot excitons are usually neglected in optical spectroscopy except in dynamics study¹⁶ for the sake of momentum conservation, as the majority of hot excitons are out of light cone. Figure 1 depicts the photoluminescence (PL) process in TMDs. The excited electrons and holes immediately form excitons in a highly non-equilibrium state once pumped as the Fig.1(a) elaborates. After a time τ_{th} (\sim sub-100fs),^{17, 18} a thermalization among excitons themselves is reached and excitons follow the Boson/Boltzmann distribution characterized with the exciton temperature $T_{exciton}$ (Fig.1(b)). Note that the exciton temperature is still much higher than the lattice temperature $T_{lattice}$ at this time. The excitons further cool down accompanying with an energy transfer to lattice via exciton-phonon scattering or some other process^{19, 20, 21} until achieving thermal equilibrium ($T_{exciton} = T_{lattice}$), characterized by a time scale τ_{ex-ph} (\sim tens of picosecond).^{16, 22, 23, 24, 25}

It is widely assumed that excitons and lattice share the same temperature in optical spectroscopy. Given that the excitons' radiative lifetime of sub-picosecond²⁶ is much shorter than τ_{ex-ph} , the excitons could radiate before thermalizing with the lattice. Meanwhile, only the excitons inside the light cone can realize direct radiative recombination for the requirement of in-plane momentum conservation (Fig.1(d)). Intuitively, the temperature of excitons seems not as important as that of electrons since these radiation-active excitons are much less influenced by the exciton temperature. The homogeneous linewidth broadening (\sim several meV) can also relax to some extent the energy-momentum conservation requirement in exciton's light emission²⁷. We calculate the PL spectra at various exciton temperatures ($T_{exciton}$) and conclude this homogeneous linewidth broadening effect is considerably minor and has a negligible contribution to the PL linewidth (more specifically in SI). The other mechanism accounting for the linewidth broadening is the acoustic phonon assisted exciton photoluminescence^{28, 29, 30}. The hot excitons (green circle in Fig.1(d)) could be scattered into the light cone by absorbing or emitting acoustic phonons.

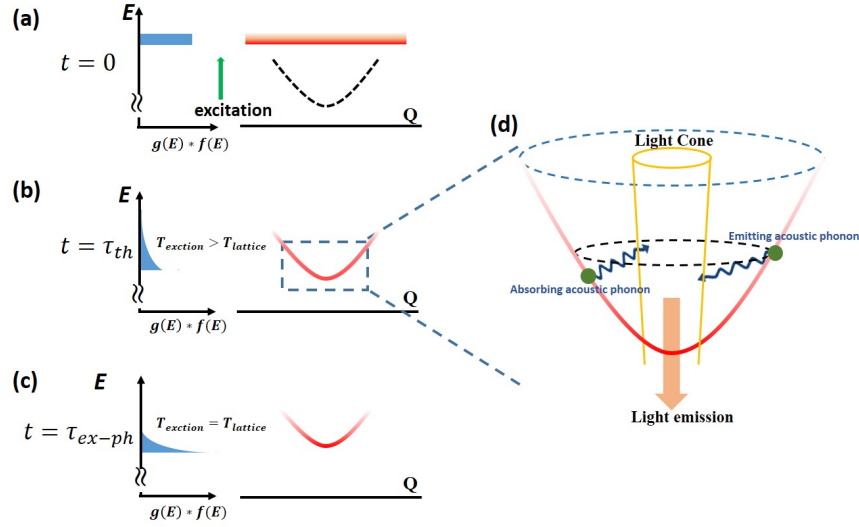


Figure 1: Schematic of the exciton distribution dynamics. (a) at $t = 0$, excitons are in a highly non-equilibrium state after a pulse excitation. (b) at $t = \tau_{th}$, the excitons reach thermalisation of themselves at $T_{exciton} > T_{lattice}$. (c) at $t = \tau_{ex-ph}$, the exciton temperature cools down and achieves a thermal equilibrium with lattice. $g(E)$ and $f(E)$ represent the density of states and Boltzmann distribution respectively. Q is the center of mass momentum of excitons. The line-thickness of the exciton dispersion (in red) represents the effective occupation. (d) Zoom-in of the dashed area in (b) sketches acoustic phonon assisted exciton photoluminescence.

In this letter, we elaborate the contribution of hot excitons to optical properties of monolayer MoSe_2 . With the intensity-dependent, temperature-dependent PL and PLE experiments combined with the simulations, we experimentally distinguish the influences of the exciton temperature and the lattice temperature in the PL spectrum. It is concluded that the acoustic phonon assisted photoluminescence accounts for the non-Lorentzian high-energy tail in the PL spectrum and the hot exciton effect is significant to optical properties of TMDs. Besides, the contrasting linewidth broadening behaviors owing to exciton temperature increase or lattice temperature increase are discussed. It is experimentally demonstrated that the effective exciton temperature can be tuned by excitation energy.

Results:

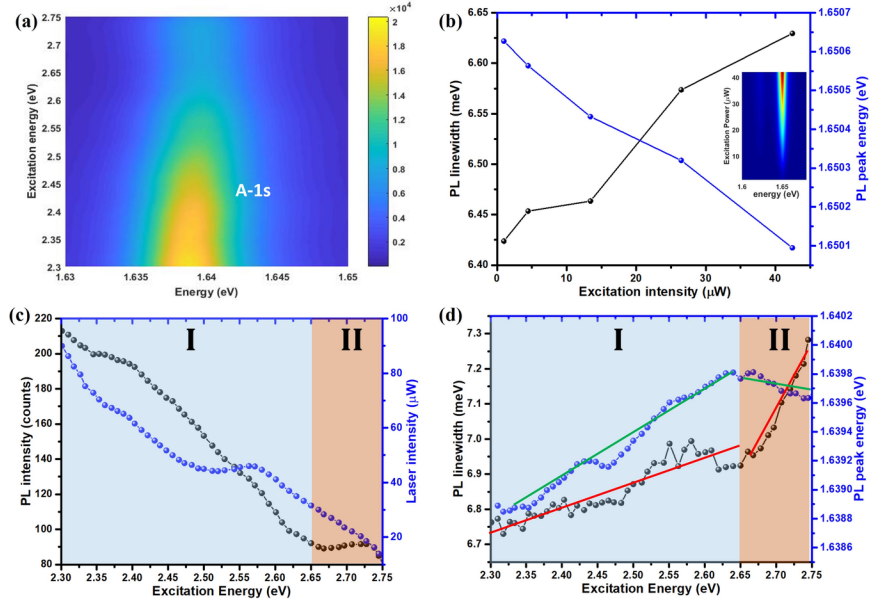


Figure 2: (a) PLE spectral map of MoSe₂ with the excitation energy ranging from 2.3eV to 2.75eV. Lorentz fitting results of (a): PL intensity (c), PL peak energy and PL linewidth (d) are summarized as a function of excitation energy. (c), (d) are further divided into two regions based on the PL intensity. (b) The PL linewidth and PL energy peak (determined by Lorentz fitting) as a function of excitation intensity. The inset shows the 2D map of excitation intensity dependent PL spectra. The excitation-intensity-dependent PL is measured under an excitation of 2.33eV at 15K.

Figure 2 summarize our PLE and excitation-intensity-dependent PL data. The excitation energy ranging from 2.3eV to 2.75eV is set far beyond the A and B exciton energies to avoid resonant absorption. The excitation intensity is kept below 100 μ W to minimize the local heating. The PL intensity across the excitation range primarily results from the corresponding excitation intensity profile (blue ball in Fig.2(c)) and the absorption coefficient (details in SI). At region I, the PL intensity decreases as the excitation energy increases primarily owing to the reduction of laser intensity (blue balls in Fig.2(c)). At region II, the PL intensity remains unchanged relatively and even slightly increases though the excitation intensity reduces with the increase energy, which may result from the boosted absorption in C band (more details in SI). The energy shift of *A-1s* exciton shows a consistent trend with PL intensity or exciton density, which also agrees well with our excitation intensity dependent PL result (Fig.2(b)). In Fig.2(b), the *A-1s* peak energy undergoes a slight redshift with the increase of exciton density under the excitation of 2.33eV accompanying with the linewidth broadening, which is consistent to the previous results³¹. The redshift is attributed to the bandgap renormalization and Coulomb screening effect. Usually, as the excitation intensity increases, the electronic bandgap decreases owing to the bandgap renormalization from photocarriers^{32, 33, 34, 35}, whereas the Coulomb screening effect is enhanced owing to the increased exciton density, leading to the decrease of the exciton binding energy, and consequently results in the PL peak energy blueshift³⁵. In monolayer MoSe₂, the bandgap renormalization effect is larger than the Coulomb screening effect and therefore the PL peak undergoes a redshift as a function of excitation intensity. Figure 2(d) indicates that the excitation energy plays a more prominent role at low exciton density. Usually, a low-intensity excitation leads to narrower exciton PL linewidth on account of the less Auger-like exciton-exciton interaction^{26, 36} as elaborated in Fig.2(b). In region I, although the PL intensity or exciton density monotonically decreases with the increasing excitation energy, the PL linewidth almost linearly increases. It seems contradictory to our excitation intensity dependent PL results (Fig.2(b)) if only the exciton density induced linewidth variation is taken in account. We attribute this linewidth broadening to the acoustic-phonon assisted photoluminescence which

we elaborate in the following section. In region II, the PL intensity remains flat and the acoustic-phonon assisted photoluminescence plays a solely role in broadening the linewidth. Hence, the PL linewidth in region II increases faster than in region I (the two red lines in Fig.2(d)). Meanwhile, the Raman scattering is exploited to monitor the lattice temperature under the excitation (below $100\mu W$), showing that the local heating is negligible and the local lattice temperature remains a constant in the excitation range (details in SI). The anomalous linewidth broadening in both regions I and II and the non-Lorentzian line shape of PL spectra are then attributed to the effective exciton temperature rise which activates the acoustic-phonon assisted photoluminescence process as demonstrated in Fig.3.

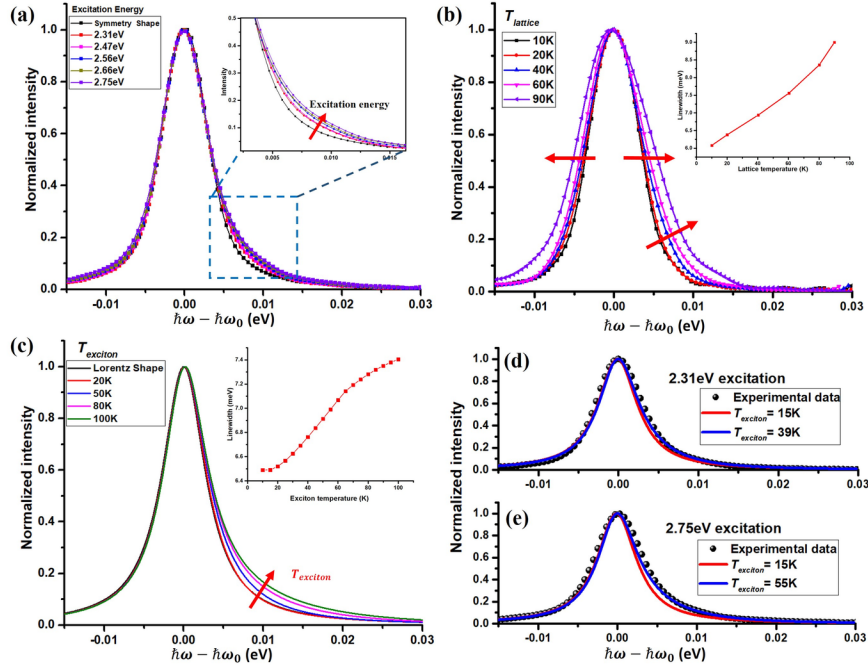
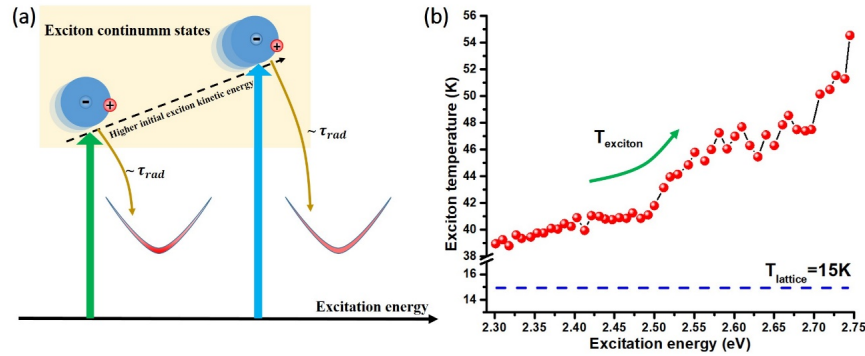


Figure 3. (a) Representative PL spectra under different excitation energies at 15K base temperature. The PL spectra are renormalized and shifted with respect to the spectral peak for comparison. The upper halves of the PL lineshape (normalized PL > 0.5) are nearly the same, and the lower parts of PL lineshape expand at the higher excitation energy. The expansion weighs heavily at the higher energy tails as magnified in the inset. (b) Representative PL spectra at various cryostat temperature. The linewidth broadening owing to the lattice temperature displays different pattern against that of exciton temperature. The inset shows the linewidth from Lorentz fitting as a function of the lattice temperature (c) Simulated PL spectra with the mechanism of acoustic phonon assisted exciton emission, where the lattice temperature is kept constant ($T_{\text{lattice}} = 15K$) and the exciton temperature is the sole variable. The high energy side tail expands obviously accompanying with the linewidth broadening. The inset shows the linewidth broadening as a function of the exciton temperature. Simulation result of PL spectra with excitation energy of 2.31eV (d) and 2.75eV (e), the exciton temperature is estimated to be 39K and 55K ($\sim 24K$ and $40K$ higher than the lattice temperature) under the excitation energies of 2.31eV and 2.75eV, respectively.

Figure 3(a) shows the representative PL spectra under different excitation energies. These PL spectra are renormalized and shifted with respect to the PL energy peak for better comparison. Note that the top halves of the PL spectra where the normalized intensity > 0.5 are nearly the same across the excitation energy range. Contrarily the tail at the high energy side expands with the elevating excitation energy as illustrated in the inset. This linewidth broadening has a contrasting manner to the lattice temperature induced line shape broadening (Figure 3(b)) which displays a whole line shape broadening other than just an expansion in

the tail. To simulate the phonon-assisted PL we set the exciton temperature as the single variable and keep lattice temperature as a constant ($\sim 15\text{K}$). Figure 3(c) shows the simulated PL spectrum of $A1s$ exciton under the acoustic phonon assisted photoluminescence mechanism with all defined parameters from M. M. Glazov and B. Urbaszek’s work²⁸ (detailed in SI). The expansion at the higher energy edge leads to the effective linewidth broadening (inset of Fig.3(c)), remarkably reproducing the experimental features in Fig.2(d). The simulation perfectly describes our experimental results and it clearly indicates that the acoustic phonon assisted photoluminescence process makes significant contribution to the whole PL spectrum in high quality samples. Comparing our experimental (Figure 3(a)) with simulation results (Fig.3(c)), we conclude that the higher excitation energy leads to the higher exciton temperature and finally raises non-Lorentz high energy tail. As demonstrated in the Fig.3(d) and (e), the effective exciton temperature (T_{exciton}) is 24K higher than the lattice temperature (T_{lattice}) when the excitation is at 2.31eV and 40K higher at 2.75eV , respectively.



Under higher energy excitation, excitons will have higher initial kinetic energy¹⁷. Within a typical exciton radiative lifetime τ_{rad} , the exciton reaches an effective exciton temperature (T_{exciton}) which is significantly different from the lattice temperature as sketched in Fig.4(a). In Fig.4(b), the effective exciton temperature is retrieved from the fitting of our PL spectra based on our model which incorporates two components: one is the Lorentz function which describes the PL from the exciton inside the light cone; the other is the high-energy tale as elaborated in the SI-Note 6 which describes the acoustic phonon assisted PL (T_{exciton} as a fitting parameter) from excitons outside the light cone. The latter contributes more weight as the T_{exciton} increases. Our PLE experiments indicate that the effective exciton temperature can be tuned continuously by the excitation energy as shown in the Fig.4(b).

Figure 4 (a) Sketch of the relation between the effective exciton temperature and the excitation energy. The exciton excited by higher energy photon has a higher initial kinetic energy. After a time scale ($\sim \tau_{\text{rad}}$), the excitons reach different effective exciton temperature. (b) The effective exciton temperature as a function of the excitation energy.

In summary, our PL and PLE spectroscopic experiments reveal that the effect of hot excitons and the effective exciton temperature can be remarkably extracted from the PL spectrum of monolayer TMDs. We elaborate the roles of effective exciton temperature and lattice temperature in photoluminescence spectra and the linewidth broadening mechanism. The thermal equilibrium between the excitons and the lattice is not necessarily achieved in linear optical properties of 2D TMDs. The effective exciton temperature could be tuned by excitation energy.

Methods:

Crystal growth

Bulk MoSe_2 crystals are grown by the chemical vapor transport (CVT) method. Mo powder (99.9%), slightly excessive Se ingot (99.999%), and a bit of iodine as transport agents are loaded in silica tubes, which are evacuated and sealed. Then, the silicon tubes are put in the reaction zone of 950 and the growth zone of

900 . After fifteen days, bulk MoSe₂ with large size are obtained in the cold zone. The monolayer MoSe₂ is mechanically exfoliated onto Si substrate with 285 nm SiO₂ film.

Sample preparation:

Monolayer MoSe₂ and thin hBN were first exfoliated from bulk MoSe₂ crystal onto the different Si/SiO₂(300nm) substrates. Afterwards, dry-transfer technique was used to stack them together. Fig.S1 shows the optical image of our hBN encapsulated MoSe₂ under bright and dark field.

PLE measurement:

In our PLE measurement, the light source (SuperK EXTREME EXB-3, NKT photonics) is a picosecond laser (80MHz, 5ps) pumped supercontinuum photonic crystal fiber going through a motorized continuous band-pass filter. The PL is collected through long working distance objective (Olympus, 50x) with a spectrometer (Shamrock 193i) and an electron-multiplying charge-couple-device (EMCCD, Andor).

1. Chernikov A, *et al.* Exciton binding energy and nonhydrogenic Rydberg series in monolayer WS₂. *Physical review letters* **113** , 076802 (2014).
2. Ye Z, *et al.* Probing excitonic dark states in single-layer tungsten disulphide. *Nature* **513** , 214-218 (2014).
3. Ugeda MM, *et al.* Giant bandgap renormalization and excitonic effects in a monolayer transition metal dichalcogenide semiconductor. *Nature materials* **13** , 1091-1095 (2014).
4. Zhu B, Chen X, Cui X. Exciton binding energy of monolayer WS₂. *Scientific reports* **5** , (2015).
5. He K, *et al.* Tightly bound excitons in monolayer WSe₂. *Physical review letters* **113** , 026803 (2014).
6. Wang G, *et al.* Giant enhancement of the optical second-harmonic emission of WSe₂ monolayers by laser excitation at exciton resonances. *Physical review letters* **114** , 097403 (2015).
7. Mak KF, He K, Shan J, Heinz TF. Control of valley polarization in monolayer MoS₂ by optical helicity. *Nature nanotechnology* **7** , 494-498 (2012).
8. Zeng H, Dai J, Yao W, Xiao D, Cui X. Valley polarization in MoS₂ monolayers by optical pumping. *Nature nanotechnology* **7** , 490-493 (2012).
9. Wang Z, *et al.* Evidence of high-temperature exciton condensation in two-dimensional atomic double layers. *Nature* **574** , 76-80 (2019).
10. Sidler M, *et al.* Fermi polaron-polaritons in charge-tunable atomically thin semiconductors. *Nature Physics* **13** , 255-261 (2017).
11. Zhang Y, *et al.* Direct observation of the transition from indirect to direct bandgap in atomically thin epitaxial MoSe₂. *Nature nanotechnology* **9** , 111-115 (2014).
12. Kormányos A, *et al.* k-ptheory for two-dimensional transition metal dichalcogenide semiconductors. *2D Materials* **2** , (2015).
13. Wellstood F, Urbina C, Clarke J. Hot-electron effects in metals. *Physical Review B* **49** , 5942 (1994).
14. Chen Y, Li Y, Zhao Y, Zhou H, Zhu H. Highly efficient hot electron harvesting from graphene before electron-hole thermalization. *Science advances* **5** , eaax9958 (2019).
15. Cortés E, *et al.* Plasmonic hot electron transport drives nano-localized chemistry. *Nature communications* **8** , 1-10 (2017).
16. Yan T, Yu H, Xiao K, Yao W, Cui X. Probing the exciton k-space dynamics in monolayer tungsten diselenides. *2D Materials* **6** , 025035 (2019).

17. Trovatiello C, *et al.* The ultrafast onset of exciton formation in 2D semiconductors. *Nature communications* **11** , 1-8 (2020).
18. Wallauer R, *et al.* Momentum-Resolved Observation of Exciton Formation Dynamics in Monolayer WS₂. *Nano Letters* **21** , 5867-5873 (2021).
19. Hägele D, *et al.* Cooling dynamics of excitons in GaN. *Physical Review B* **59** , R7797 (1999).
20. Wang L, *et al.* Slow cooling and efficient extraction of C-exciton hot carriers in MoS₂ monolayer. *Nature communications* **8** , 1-8 (2017).
21. Kumar M, *et al.* Hot exciton cooling and multiple exciton generation in PbSe quantum dots. *Physical Chemistry Chemical Physics* **18** , 31107-31114 (2016).
22. Hohlfeld J, Wellershoff S-S, Güdde J, Conrad U, Jähnke V, Matthias E. Electron and lattice dynamics following optical excitation of metals. *Chemical Physics* **251** , 237-258 (2000).
23. Damen T, Leo K, Shah J, Cunningham J. Spin relaxation and thermalization of excitons in GaAs quantum wells. *Applied physics letters* **58** , 1902-1904 (1991).
24. Ziaja B, Medvedev N, Tkachenko V, Maltezopoulos T, Wurth W. Time-resolved observation of band-gap shrinking and electron-lattice thermalization within X-ray excited gallium arsenide. *Scientific reports* **5** , 1-7 (2015).
25. Umlauff M, *et al.* Direct observation of free-exciton thermalization in quantum-well structures. *Physical Review B* **57** , 1390 (1998).
26. Moody G, *et al.* Intrinsic homogeneous linewidth and broadening mechanisms of excitons in monolayer transition metal dichalcogenides. *Nature communications* **6** , 1-6 (2015).
27. Gupta G, Majumdar K. Fundamental exciton linewidth broadening in monolayer transition metal dichalcogenides. *Physical Review B* **99** , 085412 (2019).
28. Shree S, *et al.* Observation of exciton-phonon coupling in MoSe₂ monolayers. *Physical Review B* **98** , 035302 (2018).
29. Chow CM, *et al.* Phonon-assisted oscillatory exciton dynamics in monolayer MoSe₂. *npj 2D Materials and Applications* **1** , 1-6 (2017).
30. Helmrich S, *et al.* Phonon-Assisted Intervalley Scattering Determines Ultrafast Exciton Dynamics in MoSe₂ Bilayers. *Physical Review Letters* **127** , 157403 (2021).
31. Lorchat E, *et al.* Filtering the photoluminescence spectra of atomically thin semiconductors with graphene. *Nature nanotechnology* **15** , 283-288 (2020).
32. Cunningham PD, Hanbicki AT, McCreary KM, Jonker BT. Photoinduced bandgap renormalization and exciton binding energy reduction in WS₂. *ACS nano* **11** , 12601-12608 (2017).
33. Pogna EA, *et al.* Photo-induced bandgap renormalization governs the ultrafast response of single-layer MoS₂. *ACS nano* **10** , 1182-1188 (2016).
34. Liu F, Ziffer ME, Hansen KR, Wang J, Zhu X. Direct determination of band-gap renormalization in the photoexcited monolayer MoS₂. *Physical review letters* **122** , 246803 (2019).
35. Qiu Z, *et al.* Giant gate-tunable bandgap renormalization and excitonic effects in a 2D semiconductor. *Science advances* **5** , eaaw2347 (2019).
36. Schaibley JR, *et al.* Population Pulsation Resonances of Excitons in Monolayer MoSe₂ with Sub-1 μ eV Linewidths. *Physical review letters* **114** , 137402 (2015).

Acknowledgement:

The work was supported by the Hong Kong University Grants Council/ Research grants council under schemes of (AoE/P-701/20), GRF (17300520) and AoE seed fund of University of Hong Kong and National Key R&D Program of China (2020YFA0309600). K.W. and T.T. acknowledge support from the Elemental Strategy Initiative conducted by the MEXT, Japan (Grant Number JPMXP0112101001) and JSPS KAKENHI (Grant Numbers 19H05790, 20H00354 and 21H05233). R.D and Z.L. acknowledge support from the Singapore Ministry of Education Tier 3 Programme “Geometrical Quantum Materials” AcRF Tier 3 (MOE2018-T3-1-002), AcRF Tier 2 (MOE2019-T2-2-105). The authors thank Dr. Fengren Fan, Dr. Tengfei Yan, Dr. Bairen Zhu for fruitful discussion.

CONFLICT OF INTEREST:

Wang Yao is a co-author of the manuscript and an editor of Natural Sciences and was not involved at the handling of the peer-review process of this submission.

Author contributions

K. X. performed the experiments and analyzed the data. R. D. and Z. L. provided high quality MoSe₂ crystal. K.W. and T.T provided boron nitride crystals. W. Y. provided theoretical support. K.X. performed the simulation. X. C. supervised the project. K. X. and X. C. wrote the manuscript with the aid of all the co-authors.